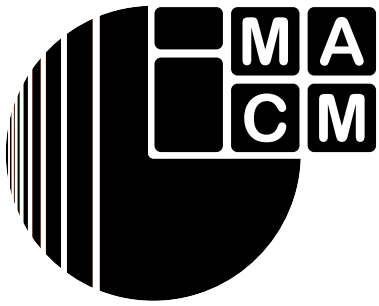


Bergische Universität Wuppertal

Fachbereich Mathematik und Naturwissenschaften

Institute of Mathematical Modelling, Analysis and Computational Mathematics (IMACM)

Preprint BUW-IMACM 12/17

Long Teng, Matthias Ehrhardt and Michael Günther

# Numerical Evaluation of Complex Logarithms in the Cox-Ingersoll-Ross Model

August 2012

http://www.math.uni-wuppertal.de

# Numerical Evaluation of Complex Logarithms in the Cox-Ingersoll-Ross Model

L. TENG, M. EHRHARDT, M. GÜNTHER

Lehrstuhl für Angewandte Mathematik und Numerische Analysis, Fachbereich C – Mathematik und Naturwissenschaften, Bergische Universität Wuppertal, Gaußstr. 20, 42119 Wuppertal, Germany,
{teng, ehrhardt, guenther}@math.uni-wuppertal.de

## Abstract

The Cox-Ingersoll-Ross (CIR) model has been a benchmark in finance for many years because of its analytical and structural tractability. The wide applications and extensions of the CIR model requires to evaluate the cumulative distribution function (CDF) of the integrated CIR process in financial modelling. Usually the characteristic function of the integrated CIR process is known analytically and one can use the option pricing method of Carr and Madan to transform it to the corresponding CDF.

This characteristic function is defined via complex logarithms which often leads to numerical instabilities when it is integrated using the inverse Fourier transform. Typically, this instability is expected to be apparent for wide ranges of model parameters.

In this work, we adapt the recent approach by Kahl and Jäckel for the Heston model to deal with such instability problems. Our new strategy allows to construct a very robust routine to determine numerically a highly accurate CDF of the integrated CIR process for almost any choices of parameters.

## 1 Introduction

The Cox-Ingersoll-Ross (CIR) model [4] is one of the best known models of stochastic interest rates. The interest-rate dynamics described by this stochastic differential equation (SDE) is realistic because interest rates are always positive and shuttle around a long-term mean. Furthermore, the CIR model is applied for stochastic intensity in credit derivates. For example, Brigo and Chourdakis [1] used the CIR process to model the default intensity of the counterparty in Credit Default Swaps (CDS). In that model we need to know the cumulative distribution function (CDF) of the integrated CIR process for the numerical integration procedure.

Intuitively, the CDF of the integrated CIR process can be transformed with the approach of Carr and Madan [3] for numerically determining the option values using the Fast Fourier Transform (FFT) from the corresponding (analytically known) characteristic function. Since the characteristic function is given, an analytic expression for the Fourier transformed probability density can be developed and then numerically solved using FFT techniques. Unfortunately, we must satisfy a restriction between the grid size for infinitesimal summands and the output grid size when applying the FFT.

Chourdakis [2] adapted this methodology proposing the fractional Fast Fourier Transform (FRFT) instead of the FFT for the purpose of removing the grid sizes restriction. Jointly with the FRFT the so called control parameter (dampening parameter) is introduced to resolve the problem of the divergence of the integrand at zero. The choice of this parameter is essential and strongly depends on the model parameters, but it is still unclear how to select an optimal dampening parameter. On the other hand, an integration of the characteristic function over the infinite domain is numerically instabil due to cancellation effects and the fast growth of the characteristic function.

In this paper we adapt the approach by Kahl and Jäckel [7] for the Heston model to evaluate the CDF of the integrated CIR process. This strategy allows to construct a very robust routine to determine numerically a highly accurate CDF of the integrated CIR process for almost any choices of parameters.

# 2 The CDF of the integrated CIR

A CIR process is the process defined by a SDE of the form

$$dy_t = \kappa(\mu - y_t)dt + \sigma\sqrt{y_t}dW_t, \qquad t \geq 0, \tag{1}$$

where $\kappa$, $\mu$, $\sigma$ are positive constants and $W_t$ is a Brownian motion. We define the integrated quantity as

$$\tilde{Y}_t := \int_0^t y_s \, ds, \quad t \geq 0, \tag{2}$$

and rewrite the characteristic function of (2) $\phi_{\tilde{Y}_t}(u) = \mathbb{E}[\mathrm{e}^{iu\tilde{Y}_t}]$ under the risk-neutral probability measure

$$\phi_{\tilde{Y}_t}(u) = \mathrm{e}^{A(t,u)+B(t,u)y_0}, \tag{3}$$

with

$$A(t,u) := \frac{2\kappa\mu}{\sigma^2}\left(\ln(2) + \ln\left(\frac{\frac{b(u)}{\kappa-b(u)}\mathrm{e}^{\frac{(\kappa+b(u))t}{2}}}{a(u)\mathrm{e}^{b(u)t}-1}\right)\right), \tag{4}$$

$$B(t,u) := \frac{2ui}{\kappa - b(u)}\left(\frac{\mathrm{e}^{b(u)t}-1}{a(u)\mathrm{e}^{b(u)t}-1}\right) \tag{5}$$

where $i$ denotes the imaginary unit and with the auxiliary functions

$$a(u) := \frac{\kappa + b(u)}{\kappa - b(u)}, \qquad b(u) := \sqrt[+]{\kappa^2 - 2\sigma^2 ui}. \tag{6}$$

Here, $\sqrt[+]{\ }$ denotes the branch of the square root with positive real part.

Using an inverse Fourier transform we obtain the probability density function of the integrated CIR process as

$$f(\tilde{y}_t) := \int_0^\infty \frac{\mathrm{Re}[\mathrm{e}^{-iu\tilde{y}_t}\phi_{\tilde{Y}_t}(u)]}{\pi}\, du. \tag{7}$$

Many authors determined the corresponding CDF numerically using

$$F_{\tilde{Y}_t}(\tilde{y}_t) := \frac{1}{2} - \frac{1}{\pi}\int_0^\infty g(u)\,du, \tag{8}$$

where the function $g$ is defined as

$$g(u) := \mathrm{Re}\left[\frac{\mathrm{e}^{-iu\tilde{y}_t}\phi_{\tilde{Y}_t}(u)}{iu}\right]. \tag{9}$$

Apparently, the fact that the integrand (9) diverges at $u = 0$ leads to a cumbersome numerical integration. We further observe that the numerical integration is made even more complicated by the fact that this integrand (9) can be highly oscillatory depending on the choice of parameters. Besides, the fast growth of the characteristic function (3) is hard to handle in general, because it depends strongly on the model parameters. Therefore, a simple quadrature or a naive numerical integration is not appropriate for the integration in (8) and we show in the sequel how to apply the adaptive Gauss-Lobatto quadrature [6].

However, in order to use the adaptive Gauss-Lobatto quadrature we need to solve two problems. First, this Gauss-Lobatto algorithm is designed only to operate on finite intervals. Secondly, another problem is the complication in the calculation of the embedded complex logarithms in equation (4) when the function $g$ is evaluated repeatedly in this quadrature scheme. In the remainder of this paper, we show in Section 3 how to solve the first problem and turn in Section 4 to the second problem.

# 3 The Transformation to a Finite Interval

In this section we show how to transform the original unbounded domain of integration $[0, \infty)$ in (8) to the finite interval $[0, 1]$ for applying later the Gauss-Lobatto quadrature. This transformation relies on the asymptotic behaviour of the integrand for $u \to \infty$, see Proposition 3.1. This transformation strategy leads to an improved stability of the adaptive quadrature scheme, cf. [7]. Besides, this modified integration scheme is significantly more efficient since less quadrature points for the evaluation are needed.

**Proposition 3.1.** *For the CIR model parameters $\kappa$, $\mu$, $\sigma$, $t > 0$ we obtain the asymptotics:*

$$\lim_{u\to\infty} \frac{b(u)}{\sqrt{u}} = \sqrt{2}\sigma\, e^{\frac{7\pi}{4}i}, \tag{10}$$

$$\lim_{u\to\infty} a(u) = -1, \tag{11}$$

$$\lim_{u\to\infty} \frac{A(u)}{\sqrt{u}} = -\frac{\sqrt{2}\kappa\mu t}{\sigma}\, e^{\frac{7\pi}{4}i}, \tag{12}$$

$$\lim_{u\to\infty} \frac{B(u)}{\sqrt{u}} = \frac{\sqrt{2}i}{\sigma}\, e^{-\frac{7\pi}{4}i}. \tag{13}$$

*The proof can be found in the Appendix.*

**Proposition 3.2.** *For the CIR model parameters $\kappa$, $\mu$, $\sigma$, $t > 0$ we obtain the asymptotics for the function $g = g(u)$ defined in (9):*

$$\lim_{u\to\infty} g(u) \approx \exp^{-\sqrt{u}A_\infty} \cdot \mathrm{Re}\left(\frac{e^{-iu\tilde{y}_t + i\sqrt{u}t_\infty}}{iu}\right) = e^{-\sqrt{u}A_\infty} \cdot \frac{sin(\sqrt{u}t_\infty - u\tilde{y}_t)}{u}, \tag{14}$$

*with*

$$A_\infty = t_\infty = \frac{\kappa\mu t + y_0}{\sigma}. \tag{15}$$

*The proof follows immediately from Proposition 3.1.*

Obviously $A_\infty$ is positive and from the equation (14) we can see that the integrand $g$ defined in (9) has at least exponential asymptotic decay for $u \to \infty$. Hence, we simply transform the integration interval in (8) as

$$\int_0^\infty g(u)\, du = \int_0^1 \frac{g(u(x))}{xA_\infty}\, dx \tag{16}$$

with

$$u(x) := -\frac{\ln x}{A_\infty}. \tag{17}$$

Up to now we have achieved the desired transformation to a finite integration interval, the second issue is the choice of the branch of the multivalued complex logarithm embedded in $A(t, u)$ in (4) for calculations based on the inverse Fourier transform (8) of the function $g$. However, the restriction on the choice to the principal branch leads to a discontinuous function (9), which would lead to incorrect results. In the next section we address this issue, namely we will guarantee the continuity of the function $g$ in (16).

# 4 Numerical Evaluation of Complex Logarithms

First, let us recall that the function $g(u)$ has discontinuities if we simply select the principal branch of the complex logarithm in $A(t, u)$. In Figure 1 we first present the imaginary part of the function $A(t, u)$ as defined in (4), the discontinuities are very clearly.

In particular, it is even worse for $t = 20$ and this observation explains why a simple approach for the integration in (8) must fail, since the integrands strongly depend on the chosen parameters. Figure 2 shows the function $g(u)$ which is implemented using its respective function $A(t, u)$, see Figure 1. For $t = 20$, the discontinuous peaks of the function $g(u)$ are apparent, from its plot we can deduce that the integration of it will be very cumbersome. Besides, we can also observe a discontinuity of the function $g$ with $t = 2$ when the variable $u$ equals that value in the interval $[40, 45]$.

In order to avoid the discontinuity of the function $g$ we use the approach of Kahl and Jäckel [7] that was originally designed for the Heston model. To do so, we rewrite the characteristic function $\phi_{\tilde{Y}_t}(u)$ of the integrated CIR process defined in (3) as

$$\phi_{\tilde{Y}_t}(u) = 2^\alpha C(t, u)^\alpha \mathrm{e}^{B(t,u)y_0} \tag{18}$$

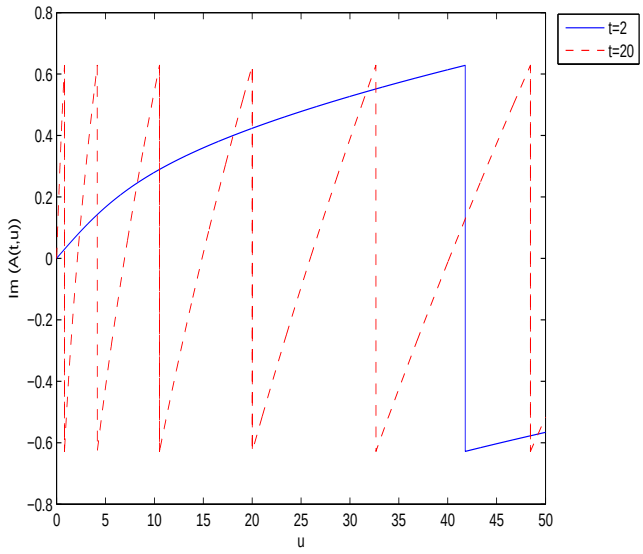


Figure 1: The function $A(t,u)$ defined in (4) with $\kappa = 0.5$, $\mu = 0.05$, $\sigma = 0.5$, $y_0 = 0.03$, implementation using the principal branch, blue curve: $t = 2$, red dashed curve: $t = 20$.

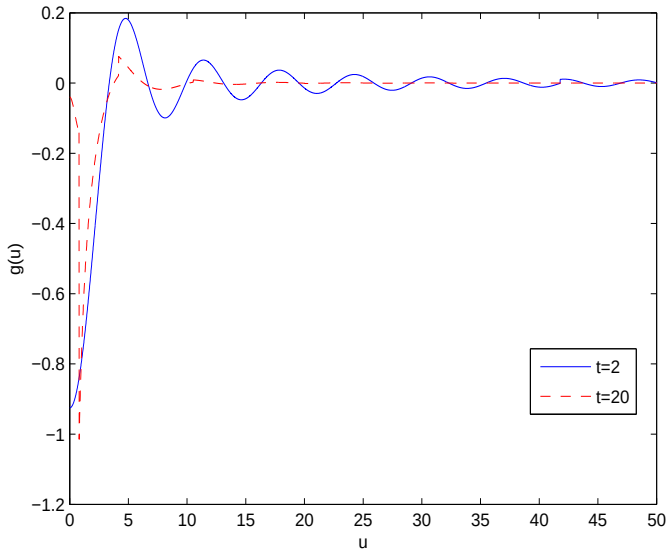


Figure 2: The function $g(u)$ defined in (9) with $\kappa = 0.5$, $\mu = 0.05$, $\sigma = 0.5$, $\tilde{y}_t = 1$, $y_0 = 0.03$, implementation using the principal branch, blue curve: $t = 2$, red dashed curve: $t = 20$.

where

$$A(t,u) = \alpha \ln 2 + \alpha \ln C(t,u), \tag{19}$$

$$\alpha := \frac{2\kappa\mu}{\sigma^2}, \tag{20}$$

$$c(u) := \frac{b(u)}{\kappa - b(u)}, \tag{21}$$

$$C(t,u) := \frac{c(u)\mathrm{e}^{\frac{(\kappa+b(u))t}{2}}}{a(u)\mathrm{e}^{b(u)t} - 1}. \tag{22}$$

From (18) we realize that we just shifted the problem from the complex logarithm to the evaluation of $C(t,u)^\alpha$; the evaluation of a complex logarithm is not necessary any more. Now it is easy to see that the function $C(t,u)^\alpha$ is exact part of the function $g$ as defined in (9) where the jump arises, because its argument $\arg(C)$ must have a discontinuity for any branch we selected. In other words, the branch switching of the complex logarithm is in fact not the main problem that gives rise to the jumps of the function $g$. For further details we refer the interested reader to [7].

In the literature different authors [8–10] proposed the straight forward idea to bookmark of the number of jumps of $C(t,u)$ between two neighbouring quadrature points. However, in our case this may lead to a rather complicated routine since we prefer to use an adaptive quadrature scheme.

In the following, we describe a relative simple procedure, originally proposed by Kahl and Jäckel [7] for the Heston model, to guarantee the continuity of $C(t,u)$ by ensuring that the argument of $C(t,u)$ is continuous, such that the discontinuity of the integrand $g(u)$ in (8) is avoided. First, we introduce the polar and the rectangular representation for $a(u)$ and $b(u)$ as defined in (6):

$$a = r_a \mathrm{e}^{i\theta_a}, \tag{23}$$

$$b = p_b + iq_b. \tag{24}$$

Then the denominator of $C(t,u)$ in (22) can be written as

$$a\mathrm{e}^{bt} - 1 = r_a \mathrm{e}^{i\theta_a + p_b t + iq_b t} - 1, \tag{25}$$

$$= r^* \mathrm{e}^{i(\chi^* + 2\pi m)}, \tag{26}$$

where

$$m := \mathrm{int}\left[\frac{\theta_a + q_b t + \pi}{2\pi}\right], \tag{27}$$

$$\chi^* := \arg(a\mathrm{e}^{bt} - 1), \tag{28}$$

$$r^* := |a\mathrm{e}^{bt} - 1|. \tag{29}$$

Note that in (27) $\mathrm{int}[\cdot]$ denotes the Gauss's integer brackets.

Restricting the argument $\theta_a \in [-\pi, \pi)$ means that we cut the complex plane along the negative real axis. When the function $C(t,u)$ in (22) crosses the negative real axis by varying $u$, the sign of the argument of $C(t,u)$ changes form $-\pi$ to $\pi$ and therefore the

argument of $C(t,u)^\alpha$ changes from $-\pi\alpha$ to $\pi\alpha$. Then the function jumps if $\alpha$ is not an integer, since

$$e^{i\pi} = e^{-i\pi} \Rightarrow \begin{cases} e^{i\alpha\pi} = e^{-i\alpha\pi} & \text{if } \alpha \in \mathbb{Z} \\ e^{i\alpha\pi} \neq e^{-i\alpha\pi} & \text{else.} \end{cases} \tag{30}$$

In general, we can assume $\chi^*$ and $\theta_a$ to be on the same argument interval $[-\pi, \pi)$, because the subtraction of 1 from $ae^{bt}$ is simply a shift parallel to the real axis as long as $r^*$ defined in (29) never crosses the negative real axis. This essential property is guaranteed due to the following Proposition 4.1.

**Proposition 4.1.** *The absolute value of the function $ae^{bt}$ is strictly greater than 1.*

The proof is given in the Appendix.

Now we perform the same calculation with the numerator of $C(t,u)$. First we need the polar representation for $c(u)$ defined in (21):

$$c = r_c e^{i\theta_c}. \tag{31}$$

Using the representation of $b(u)$ in (24) we have

$$ce^{\frac{(\kappa+b)t}{2}} = r_c e^{i\theta_c + \frac{t}{2}(k+p_b+iq_b)} \tag{32}$$

$$= r^{**} e^{i(\chi^{**}+2\pi n)}, \tag{33}$$

with

$$n := \text{int}\left[\frac{\theta_c + \frac{t}{2}q_b + \pi}{2\pi}\right], \tag{34}$$

$$\chi^{**} := \arg(ce^{\frac{(\kappa+b)t}{2}}), \tag{35}$$

$$r^{**} := |ce^{\frac{(\kappa+b)t}{2}}|. \tag{36}$$

This situation seems to be more intuitive; both $\chi^{**}$ and $\theta_c$ can be assumed to be on the same argument interval $[-\pi, \pi)$.

So far we obtain the following representation of $C(t,u)$ by combining the results above:

$$C(t,u) = \frac{c(u)e^{\frac{(\kappa+b(u))t}{2}}}{a(u)e^{b(u)t} - 1} = \frac{r^{**}}{r^*} e^{i(\chi^{**} - \chi^* + 2\pi(n-m))}, \tag{37}$$

and the rotation count correction

$$\ln C(t,u) = \ln\left(\frac{r^{**}}{r^*}\right) + i(\chi^{**} - \chi^* + 2\pi(n-m)). \tag{38}$$

By comparing the results with and without the rotation count correction (38) in Figure 3 we observe that the jump discontinuities can be removed.

Now, we will consider the function $g(u)$ from Figure 2 and apply the rotation count correction. First we look at the $g(u)$ which is smoother, namely only a discontinuity in the interval $[40, 45]$ as we have mentioned before, see Figure 4.

In Figure 5 we compare the functions $g(u)$ with and without rotation count correction which are initialized with a high level of the CIR model parameter, in this case the function has worse discontinuities. Let us note that high levels refer to the situations when the maturity of the CIR process is large, here $t = 20$.

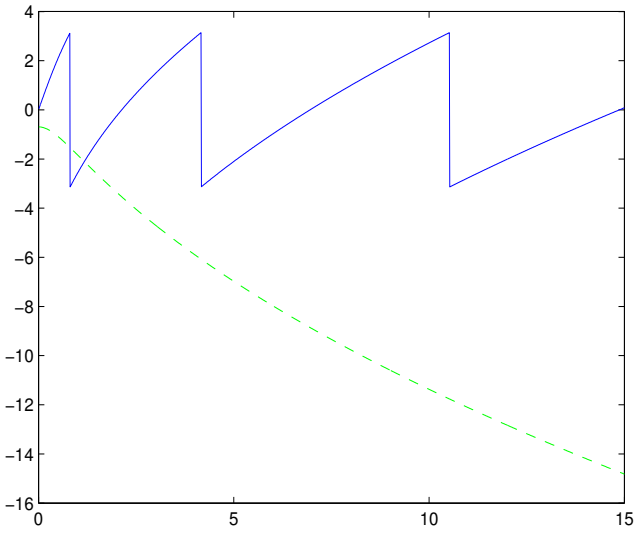


Figure 3: The blue solid curve is the argument of $C(t,u)$ as defined in (22) by using just the principal branch of $C(t,u)$ and the green dashed one is also the argument of $C(t,u)$ but with the rotation count correction (38) for $\kappa = 0.5$, $\mu = 0.05$, $\sigma = 0.5$, $y_0 = 0.03$.

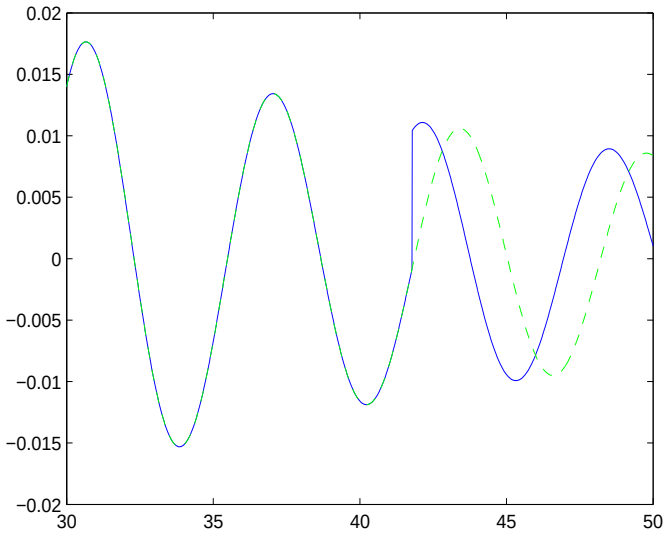


Figure 4: The blue solid curve is exactly a zoomed region of $g(u)$ (blue) shown in Figure 2 for $u \in [30, 50]$, the green dashed curve is obtained with the rotation count correction (38).

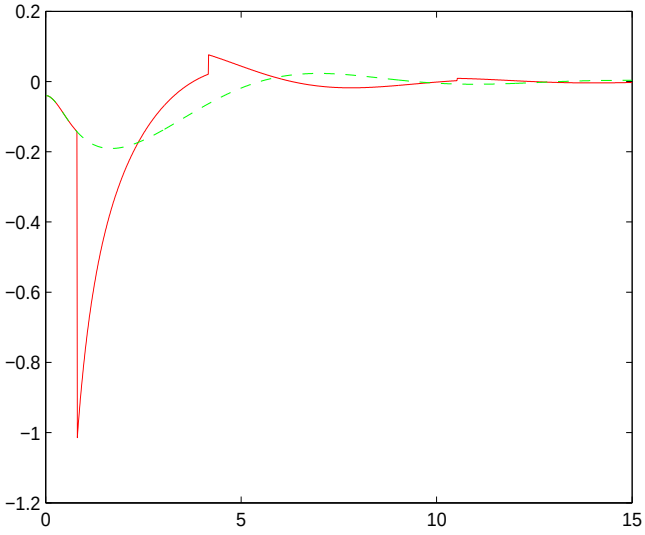


Figure 5: The red solid curve is exactly the function $g(u)$ (red) shown in Figure 2 for $u \in [0, 15]$, the green dashed curve is obtained with the rotation count correction (38).

# 5 The Quadrature on the Finite Interval

We rewrite the CDF as defined in (8) using the transform (16) as

$$F_{\tilde{Y}_t}(\tilde{y}_t) = \int_0^1 \tilde{f}(x)\, dx, \tag{39}$$

where

$$\tilde{f}(x) := \frac{1}{2} - \frac{g(-\frac{\ln x}{A_\infty})}{x \cdot \pi \cdot A_\infty}. \tag{40}$$

This means that for the implementation using the adaptive Gauss-Lobatto quadrature we additionally need the limits of $\tilde{f}(x)$ at the boundaries 0 and 1 of the integral. For $x \to 0$ we observe that

$$\lim_{x \to 0} \tilde{f}(x) = \frac{1}{2}. \tag{41}$$

The function $g(u)$ is not defined at $u = 0$, but since $g(u)$ is continuous at zero, we can determine the missing value analytically:

**Proposition 5.1.** *The function*

$$g(u) = \mathrm{Re}\left[\frac{e^{-iu\tilde{y}_t}\phi_{\tilde{Y}_t}(u)}{iu}\right] \tag{42}$$

*has the following limit at zero:*

$$\lim_{u \to 0} g(u) = -\tilde{y}_t + \mathrm{Im}(A(t,0)') + \mathrm{Im}(B(t,0)') \cdot y_0, \tag{43}$$

*where*

$$\mathrm{Im}(A(t,0)') = \frac{\mu\kappa e^{-\kappa t} + \mu\kappa(t\kappa - 1)}{\kappa^2}, \tag{44}$$

*and*

$$\mathrm{Im}(B(t,0)') = \frac{1 - e^{-\kappa t}}{\kappa}. \tag{45}$$

The proof can be found in Appendix I.

Now we can implement the required Fourier inversion in (8) as a Gauss-Lobatto integration over the finite interval $[0, 1]$ instead of the infinite interval $[0, u]$ using the transformation (15)–(17). We see the first example in Figure 6.

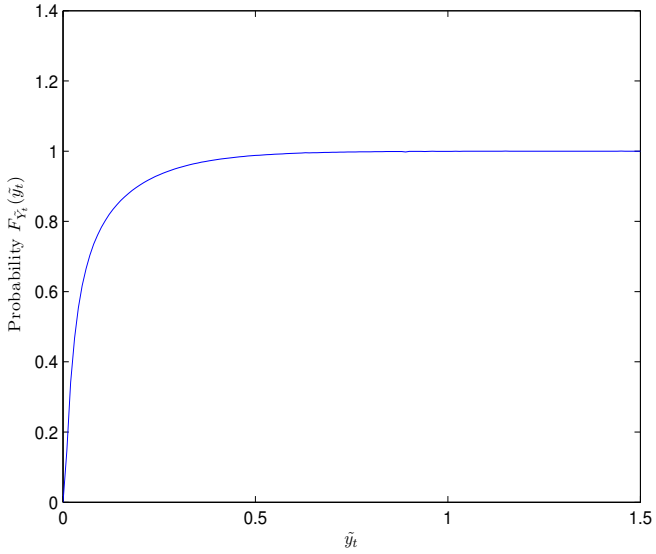


Figure 6: The CDF $F_{\tilde{Y}_t}(\tilde{y}_t)$ of the integrated CIR process $\tilde{Y}_t$ with $\kappa = 0.5$, $\mu = 0.05$, $\sigma = 0.5$, $y_0 = 0.03$, $t = 2$ computed with the adaptive Gauss-Lobatto scheme for a prescribed accuracy $10^{-6}$.

The stability of Gauss-Lobatto integration over the finite interval $[0, 1]$ grants that even extreme probabilities can be computed, like we choose a very long dated maturity $t = 30$ and see the corresponding CDF in Figure 7.

Besides, we show the CDFs of the integrated CIR processes which are computed with a lower level of parameter in Figure 8.

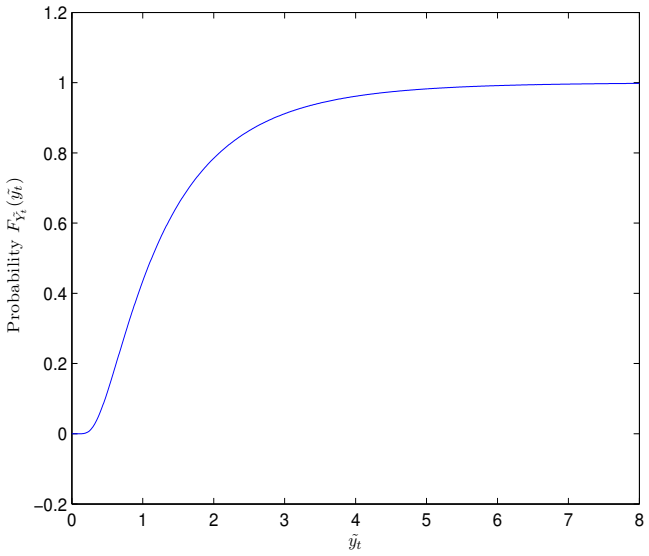


Figure 7: The CDF $F_{\tilde{Y}_t}(\tilde{y}_t)$ of the integrated CIR process $\tilde{Y}_t$ with $\kappa = 0.5$, $\mu = 0.05$, $\sigma = 0.5$, $y_0 = 0.03$, $t = 30$ computed by the adaptive Gauss-Lobatto scheme for a prescribed accuracy $10^{-6}$.

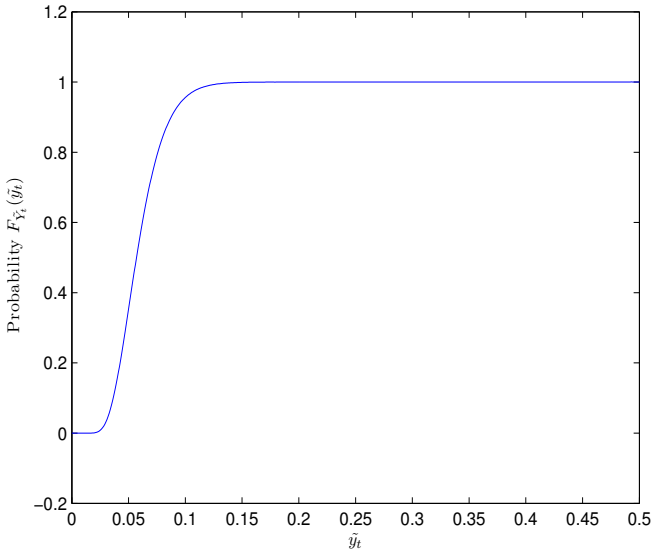


Figure 8: The CDF $F_{\tilde{Y}_t}(\tilde{y}_t)$ of the integrated CIR process $\tilde{Y}_t$ with $\kappa = 0.8$, $\mu = 0.02$, $\sigma = 0.1$, $y_0 = 0.02$, $t = 3$ computed by the adaptive Gauss-Lobatto scheme for a prescribed accuracy $10^{-7}$.

# 6 Conclusion

We adapt the numerical option pricing approach in the Heston model by Kahl and Jäckel [7] to compute probabilities from the characteristic function in the CIR model. This strategy allows us to treat properly the numerical instabilities which are typically caused by log-characteristic functions involving complex logarithms and complex power expressions.

The crucial difficulty here is to deal with the multivalued nature of the complex power function. After resolving this difficulty we obtained a very robust routine to determine numerically highly accurate CDF probabilities in the CIR model.

# References


[1] D. Brigo and K. Chourdakis, *Counterparty Risk for Credit Default Swaps: Impact of spread volatility and default correlation*, Int. J. Theoret. Appl. Fin. **12** (2009), 1007–1026.

[2] K. Chourdakis, *Option Pricing using the Fractional FFT*, J. Comput. Fin. **8** (2005), 1–18.

[3] P. Carr and D. Madan, *Option Valuation using the Fast Fourier Transform*, J. Comput. Fin. **2** (1999), 61–73.

[4] J. Cox, J. Ingersoll and S. Ross, *A Theory of the Term Structure of Interest Rates*, Econometrica **53** (1985), 385–408.

[5] R.J. Elliot and P.E. Kopp, *Mathematics of Financial Markets*, Springer, 2004.

[6] W. Gander and W. Gautschi, *Adaptive Quadrature – Revisited*, BIT **40** (2000), 84–101.

[7] C. Kahl and P. Jäckel, *Not-so-complex Logarithms in the Heston Model*, Wilmott Magazine, September 2005, 94–103.

[8] R. Lee, *Option Pricing by Transform Methods: Extensions, Unification, and Error Control*, J. Comput. Fin. **7** (2005), 51–86.

[9] R. Schöbel and J. Zhu, *Stochastic Volatility With an Ornstein Uhlenbeck Process: An Extension*, European Finance Review **3** (1999), 23–46.

[10] A. Sepp, *Pricing European-Style Options under Jump Diffusion Processes with Stochastic Volatility: Application of Fourier Transform*, Working paper, Institute of Mathematical Statistics, Faculty of Mathematics and Computer Science, University of Tartu, J. Liivi 2, 50409 Tartu, Estonia, September 2003.

# Appendix

Proposition [3.1]

*Proof.*

$$\lim_{u\to\infty}\frac{b(u)}{\sqrt{u}}=\lim_{u\to\infty}\sqrt{\frac{\kappa^2}{u}-2i\sigma^2}=\sqrt{2}\sigma\sqrt{-i}=\sqrt{2}\sigma\mathrm{e}^{\frac{7\pi}{4}i},$$

Regarding this result we have straightforward $\lim_{u\to\infty}a(u)=-1$.
Now we prove the equation (12)

$$\begin{aligned}\lim_{u\to\infty}\frac{A(u)}{\sqrt{u}}&=\lim_{u\to\infty}\frac{2\kappa\mu}{\sigma^2}\left(\ln(2)+\frac{t}{2}(\kappa-b(u))+\ln\left(\frac{-\mathrm{e}^{tb(u)}}{a(u)\mathrm{e}^{tb(u)}-1}\right)\right)/\sqrt{u}\\&=\lim_{u\to\infty}\frac{2\kappa\mu}{\sigma^2}\left(-\frac{t}{2}\frac{b(u)}{\sqrt{u}}\right)\\&=-\frac{\sqrt{2}\kappa\mu t}{\sigma}\mathrm{e}^{\frac{7\pi}{4}i}.\end{aligned}$$

Finally, we show the equation (13)

$$\begin{aligned}\lim_{u\to\infty}\frac{B(u)}{\sqrt{u}}&=\lim_{u\to\infty}\frac{2ui}{\kappa-b(u)}\left(\frac{1}{a(u)}\left(1+\frac{1-a(u)}{a(u)\mathrm{e}^{tb(u)-1}}\right)\right)/\sqrt{u}\\&=\lim_{u\to\infty}\frac{-2\sqrt{u}i}{\kappa-b(u)}\\&=\lim_{u\to\infty}\frac{2i}{\frac{b(u)}{\sqrt{u}}}=\frac{\sqrt{2}i}{\sigma}\mathrm{e}^{-\frac{7\pi}{4}i}.\end{aligned}$$

□

Proposition [4.1]

*Proof.* Since the function $\mathrm{Re}\,b(u)$ and the parameter $t$ are non-negative, we only need to prove

$$|a(u)|=\left|\frac{\kappa+b(u)}{\kappa-b(u)}\right|>1.$$

This is to say that we have to show

$$|\kappa+b(u)|^2>|\kappa-b(u)|^2. \tag{46}$$

We split $b(u)$ into a real and imaginary part as

$$b(u)=b_r+ib_i,\qquad b_r,b_i\in\mathbb{R}$$

then the left hand side of (46) satisfies

$$0<|\kappa+b(u)|^2=|\kappa+b_r+ib_i|^2=(\kappa+b_r)^2+b_i^2=\kappa^2+2\kappa b_r+|b(u)|^2$$

and analogously the right hand side of (46) fullfills

$$0<|\kappa-b(u)|^2=\kappa^2-2\kappa b_r+|b(u)|^2$$

The fact that $\kappa>0$ and $b_r>0$ completes the proof. □

Proposition [5.1]

*Proof.* Combining the function $g(u)$ with the function $\phi_{\tilde{Y}_t}(u)$ as given in (3) we have

$$\lim_{u\to 0} g(u) = \lim_{u\to 0} \mathrm{Im}\left[\mathrm{e}^{-iu\tilde{y}_t}\frac{\mathrm{e}^{A(t,u)+B(t,u)y_0}}{u}\right].$$

First we consider the limits of $a(u)$ and $b(u)$ as defined in (6)

$$\lim_{u\to 0} b(u) = |\kappa| = \kappa, \qquad \lim_{u\to 0} a(u) = \infty, \tag{47}$$

where the last step in the limit of $b(u)$ follows from the fact that the CIR model parameter $\kappa$ is always positive. From (47) we can directly deduce

$$\lim_{u\to 0} A(t,u) = \lim_{u\to 0} B(t,u) = 0, \tag{48}$$

and thus

$$\lim_{u\to 0} \mathrm{e}^{-iu\tilde{y}_t + A(t,u) + B(t,u)y_0} = 1. \tag{49}$$

Now we split the exponent in the last equation into a real and imaginary part as

$$H(u) + iJ(u) := -iu\tilde{y}_t + A(t,u) + B(t,u)y_0, \tag{50}$$

with functions $H(u)$ and $J(u) : \mathbb{R} \to \mathbb{R}$. Furthermore, from (49) we also know that

$$\lim_{u\to 0} H(u) = 0, \qquad \lim_{u\to 0} J(u) = 0.$$

Now we can calculate the value of $g(u)$ at zero as follows

$$\begin{aligned}
g(0) &= \lim_{u\to 0} \mathrm{Im}\left[\frac{\mathrm{e}^{H(u)+iJ(u)}}{u}\right] \\
&= \lim_{u\to 0} \mathrm{Im}\left[\mathrm{e}^{H(u)\frac{\cos(J(u))+i\sin(J(u)))}{u}}\right] \\
&= \lim_{u\to 0} \mathrm{e}^{H(u)\frac{\sin(J(u)))}{u}} \\
&= \lim_{u\to 0} \frac{\sin(J(u)))}{u} \\
&\overset{l'Hospital}{=} \lim_{u\to 0} J'(u)\frac{\cos(J(u))}{1} \\
&= \lim_{u\to 0} J'(u).
\end{aligned}$$

Using the equation (50) we obtain

$$g(0) = \lim_{u\to 0} J'(u) = J'(0) = \tilde{y}_t + \mathrm{Im}(A'(t,u)) + \mathrm{Im}(B'(t,u)y_0).$$

The computation of $A'(t,u)$ and $B'(t,u)$ is rather tedious but straightforward. We obtain finally

$$\begin{aligned}
\mathrm{Im}(A(t,0)') &= \frac{\mu\kappa\mathrm{e}^{-\kappa t} + \mu\kappa(t\kappa - 1)}{\kappa^2}, \\
\mathrm{Im}(B(t,0)') &= \frac{1-\mathrm{e}^{-\kappa t}}{\kappa}.
\end{aligned}$$

□